Experimental Study on Impact Absorption Capacity of Various Expanded Materials for Rock Shed

Hindawi
Shock and Vibration
Volume 2020, Article ID 7412456, 15 pages
https://doi.org/10.1155/2020/7412456

Research Article

Experimental Study on Impact Absorption Capacity of Various Expanded Materials for Rock Shed

Yusuke Kurihashi,[1] **Naochika Kogure**,[2] **Shin-ichi Nitta**,[2] **and Masato Komuro**[3]

[1]*Department of Geosciences and Civil Engineering, Kanazawa University, Kanazawa, Japan*
[2]*JSP Co., Ltd., Tokyo, Japan*
[3]*Civil Engineering Research Unit, College of Design and Manufacturing Technology, Muroran Institute of Technology, Muroran, Japan*

Correspondence should be addressed to Yusuke Kurihashi; kuri@se.kanazawa-u.ac.jp

Received 12 January 2020; Revised 13 May 2020; Accepted 14 May 2020; Published 30 May 2020

Academic Editor: Marco Lepidi

In recent years, there has been a continuous increase in the intensity of natural disasters. Slope disasters such as rock falls occur along coastlines and in mountainous regions. Rock shed structures are implemented as measures to prevent rock fall damage; however, these structures deteriorate over time, and their impact resistance also decreases. As a supplementary measure, a method employing foam material as a cushioning material has been used in practical applications. However, the effect of the compressive strength characteristics on the cushioning performance of foamed materials has not been studied thus far. Therefore, in this study, falling-weight impact-loading tests involving various fall heights were performed to examine the absorption performance of various expanded materials. Moreover, we examined the case where core slabs were layered to effectively exploit the absorption performance of the expanded materials. The results of this study are summarized as follows: (1) the transmitted impact penetration stress-strain curves right under the loading points of various expanded materials exhibit properties similar to those obtained from the results of material testing. However, in the case of expanded materials with high compressive strengths, the compressive stress from the results of material testing tends to be lower. (2) In the case of expanded materials with high compressive strengths, with and without core slabs, the distribution of the transmitted impact stress is large, and the energy absorption capacity is high. (3) In this experiment, the energy absorption capacity was found to double when core slabs are layered, regardless of the type of expanded material used. This suggests that expanded materials with high compressive strengths may contribute towards a higher improvement in energy absorption capacities, by using layered core slabs.

1. Introduction

Torrential rains occur around the world due to climate change caused by global warming, and large-scale slope disasters occur frequently. In recent years, natural disasters have continued to intensify [1]. Slope disasters such as falling rocks occur along the coast and in the mountains [2]. As road disaster prevention countermeasures against rock fall, methods such as reinforced concrete (RC) and/or pre-stressed concrete (PC) rock sheds, retaining walls, rock fall protection nets, fences, embankments, and other disaster prevention systems have been used [3]. At present, many structures have been in operation for more than 50 years. As the deterioration of structural performance due to aging may become apparent, it is necessary to urgently implement countermeasures [4].

Among them, in the case of RC/PC rock shed (Figure 1), a soil material (sand, locally generated soil, etc.) is installed as a cushioning material on the top slab to reduce the impact force caused by falling rocks [5–9]. When it is necessary to improve the impact resistance of the rock shed, a method has been applied in which the cushioning material on the top plate is replaced with a material having a high cushioning performance such as a foam material from a soil material [9–11]. Thus far, in addition to foam materials, techniques such as combining geogrids with steel materials and a three-

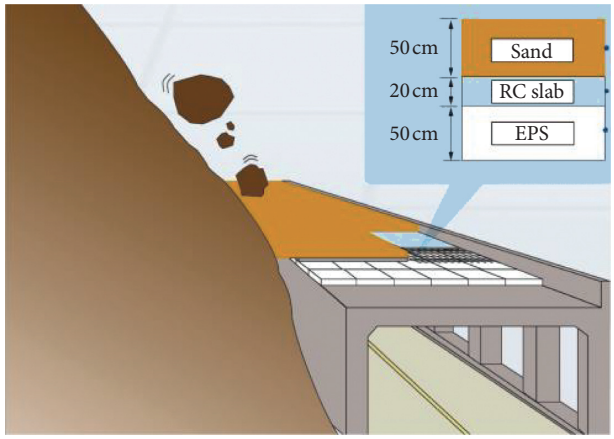

Figure 1: Outline of rock shed and cushioning materials.

layered absorption system, wherein reinforced concrete (RC) slabs and sand are installed on the foam material [9, 12] have been employed.

In recent years, foam materials with various material properties for various applications have been developed [13, 14]. In general, foam materials with high compressive strength characteristics tend to increase the transmitted impact stress when an impact load is applied and also possess high energy absorption performance. Also, when applied to the abovementioned three-layered absorption system, there is a possibility that the distribution range of transmitted impact stress can be made wider. Thus, it is considered that the use of a material with different strength characteristics from the conventional foam material may improve the absorption performance of the three-layered absorption system. However, the effect of compressive strength characteristics on the cushioning performance of foamed materials has not been studied at present.

Based on this perspective, in this study, falling-weight impact-loading tests were performed for various fall heights, with the aim of examining the absorption effects of various expanded materials with different compressive strength characteristics. Moreover, the tests were performed under the condition that the cores slabs were layered to diffuse the transmitted impact stress, to compare and examine the impacts of the compressive strength characteristics of the expanded materials on their absorption performance. We evaluated the degree of dispersion of the transmitted impact stress based on the energy conservation relationship.

2. Experiment Outline

2.1. Specimen Outline. Table 1 lists characteristics of the expanded materials for comparison used in this study. The expanded materials were polystyrene expanded material (ST), polypropylene expanded material (PP), and polyethylene-polystyrene composite expanded material (EST). The polystyrene expanded material (ST) has been widely used as a countermeasure for weak ground and reducing falling rocks in civil engineering projects thus far.

Moreover, polypropylene expanded material (PP) is superior in its dimensional stability, and it is capable of returning to its original shape even after a significant compressive deformation. Therefore, it is widely used in fenders and car bumpers. As the perseverance and compressive strength of the polyethylene-polystyrene expanded material (EST) are higher than those of other expanded materials, it is applied as a packaging material in precision apparatus and domestic electrical appliances.

Figure 2 depicts the compression test results for various expanded materials. The tests were performed for a cube with a side of 50 mm, according to ISO 884 (rigid cellular plastics—determination of compression properties) [15]. The figure indicates that the stress elastically increases to approximately 2% of compression strain in all the three expanded materials; it changes with a small increasing gradient until around 60–70% and then increases rapidly. However, the compressive stress with the same strain is different for each expanded material, which affects the transmitted impact stress when an impact load is applied.

The specimen list is presented in Table 2. A total of 22 specimens were used. The expansion material and fall height were varied for both cases, i.e., with and without core slabs. Furthermore, impact-loading tests were performed for total nine kinds of expand materials with different raw materials and the expanding magnification prior to this experiment, and materials having compressive strength characteristics that significantly differ from those of general-purpose ST expand materials were selected.

In Table 2, Term 1 of the specimen name indicates the presence of core slabs (N, without core slabs and C, with core slabs). Term 2 indicates the type of material (see Table 1), and the numeric values attached to the alphabet H of Term 3 indicate the fall height (mm).

2.2. Method and Measurement Parameter. Figure 3 shows outlines of the specimens and transmitted impact stress measurement. The plane dimension of the specimens is 240 mm on the four sides, with a thickness of 50 mm. In the case of the specimens with core slabs, a plaster board with a thickness of 12.5 mm (conforming to JIS A 6901 [16]) was installed on the expanded material. Furthermore, thickness of the plaster board was selected from specifications of the commercially available products in reference to the thickness ratio for EPS blocks and core RC slabs in three-layered absorption systems that are practically used [9].

In the weight fall impact test, a 20-kg steel weight with a tip diameter of 60 mm was allowed to free-fall from a predetermined height on the expansion material, through a linear rail. The expansion materials were installed on a steel bottom plate in which nine load cells were buried to measure the distribution of the transmitted impact stress.

Figure 4 depicts an experiment status. In the experiment, the points when the maximum penetration strain of the expanded materials exceeded 75% were defined as end states. Thus, the experiment was continued with gradually increasing falling heights until the weight penetration depth exceeded 37.5 mm (= 75% of 50 mm). This was based on the idea that (1) when a penetration strain exceeds 75%, as shown in Figure 2, the compressive stress suddenly increases and (2) the

Table 1: Material property of the expanded material.

Marks	Main component	Expanding magnification (times)	Weight of unit volume (kN/m^3)	Primary applications
ST	Polystyrene	50	0.212	Measures for land subsidence and those for reducing falling rock
PP	Polypropylene	45	0.195	Fenders and car bumpers
EST	Polyethylene-polystyrene complex	30	0.304	Cushioning material of precision apparatus and home electric appliances

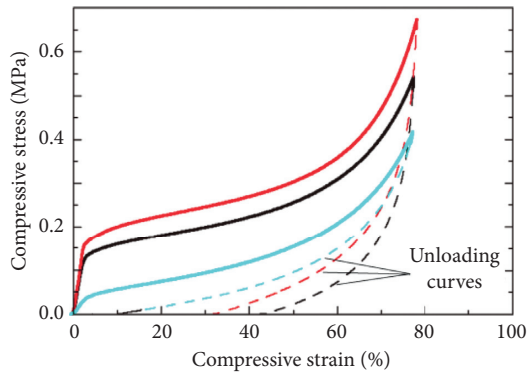

Figure 2: Results of compressive strength tests for each expanded material.

Table 2: Specimen list.

Name of specimen	Presence of core slab	Type of expanded material	Set fall height H (mm)	Measurement impact velocity V (m/s)	Input energy E_k (J)
N-ST-H50	Without core slab	ST	50	0.99	9.77
N-ST-H100			100	1.40	19.7
N-ST-H150			150	1.74	30.3
N-ST-H200			200	1.98	39.1
N-PP-H50		PP	50	0.97	9.34
N-PP-H100			100	1.40	19.7
N-PP-H150			150	1.74	30.3
N-EST-H50		EST	50	0.97	9.34
N-EST-H100			100	1.40	19.7
N-EST-H150			150	1.81	32.9
N-EST-H200			200	1.98	39.1
N-EST-H300			300	2.56	65.5
C-ST-H200	With core slab	ST	200	2.07	42.9
C-ST-H300			300	2.42	58.4
C-ST-H400			400	2.72	73.9
C-PP-H200		PP	200	1.98	39.1
C-PP-H300			300	2.56	65.5
C-EST-H200		EST	200	2.07	42.9
C-EST-H300			300	2.42	58.4
C-EST-H400			400	2.90	84.1
C-EST-H500			500	3.11	96.5
C-EST-H600			600	3.35	112.0

damage to expanded materials would become significant, as shown in Figures 5 and 6, which may lead to damage to the experimental apparatus, especially load cells (Figure 3).

The dependent variables used in this experiment are falling-weight impact, weight penetration, and transmitted impact stress distribution. The weight impact force was measured using a load cell with a capacity of 25 kN, for measuring the impact load. The quantity of weight penetration was evaluated by vertically installing a laser-type displacement meter and measuring the distance to an L-shape angle steel on the weight. The transmitted impact stress distribution was measured using load cells with a capacity of

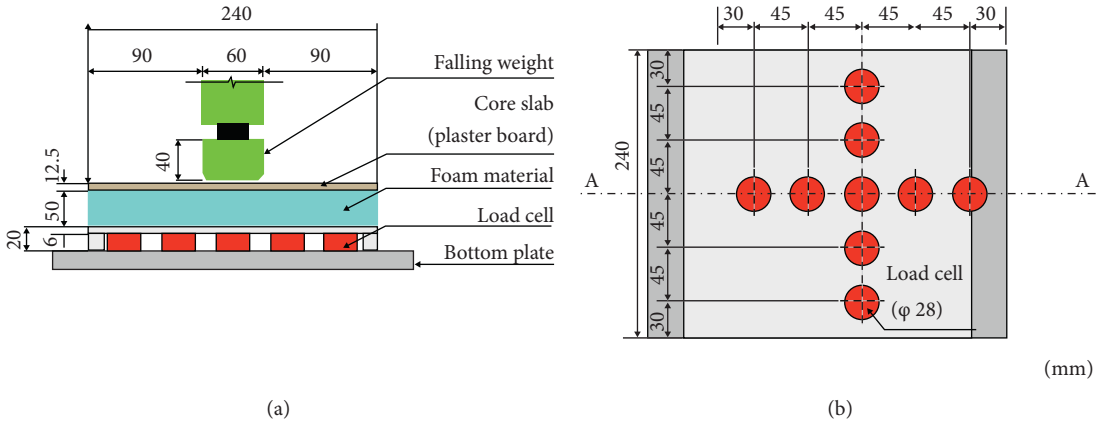

Figure 3: Outline of specimen and transmitted impact stress measurements. (a) A-A section. (b) Plan view.

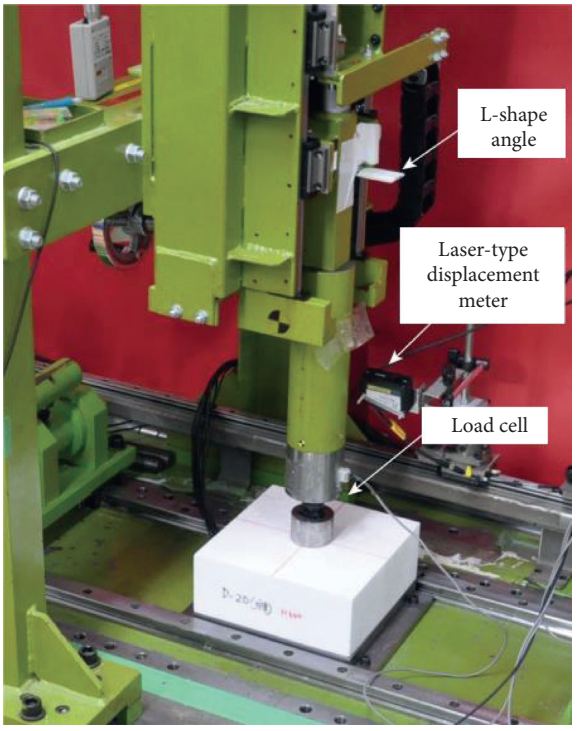

Figure 4: State of the falling-weight impact-loading test.

7 MPa; those were installed on the loading point and around it with an interval of 45 mm, as shown in Figure 3.

Moreover, the impact velocity was calculated by measuring the time required for a white plate of 30-mm length attached to the weight to pass through a laser sensor. In the experiment, these measured values were collected using a memory recorder at a sampling frequency of 2 kHz. After the experiment, the expanded materials were centrally cut to observe destruction properties.

3. Experimental Result of Expanded Material without Core Slab

3.1. Various Response Waveforms. Figure 7 shows response waveforms for each weight fall height H with respect to weight impact force, weight penetration, and transmitted impact stress right under the loading point (simply called transmitted impact stress below) of materials without core slabs. In the figure, the weight impact force presents waveform with a duration time of 50–75 ms at peak amplitudes of around 1.5–2.5 kN. Moreover, in the event that compressive strength characteristics in the abovementioned material testing are large, rising gradient and maximum impact force tend to increase while the main wave motion duration time tends to decrease.

Regarding weight penetration, the material exhibited maximum weight penetration, returned to its original state, and rebounded higher than the impact point. Moreover, the maximum weight penetration declines with the duration of main wave motion, indicating larger compressive strength

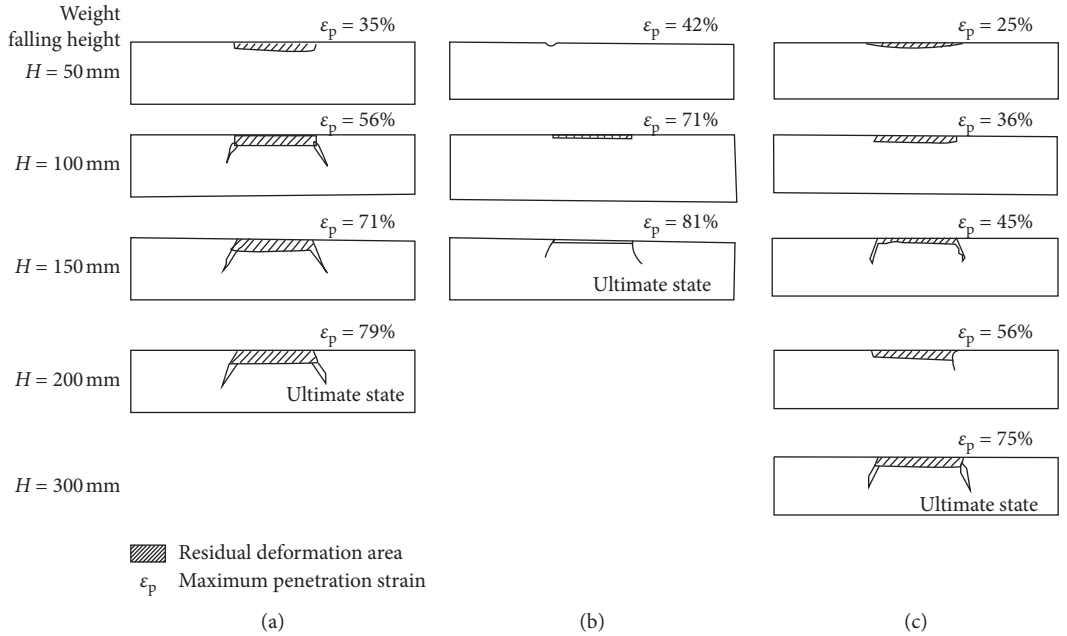

Figure 5: State of expanded material cut area in the case of material without core slabs. (a) ST. (b) PP. (c) EST.

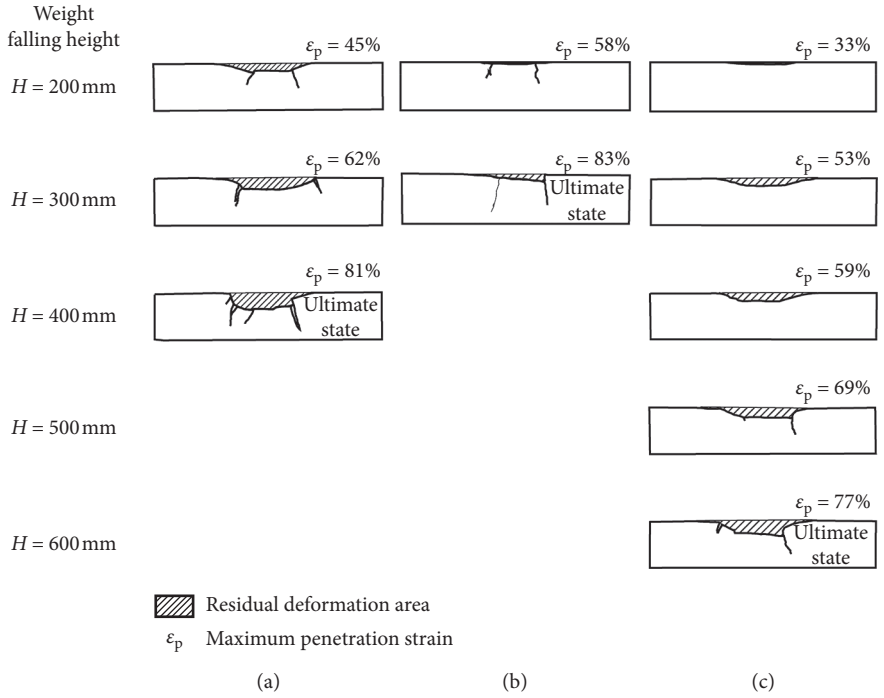

Figure 6: Cut area of the expanded material in the case with core slabs. (a) ST. (b) PP. (c) EST.

characteristics. The maximum weight penetration increased with an increase in the fall height, and the maximum fall height of the expanded materials exceeded 37.5 mm (ultimate state).

The transmitted impact stress rose suddenly with weight impact, similar to the case of the weight impact force at 20 ms of elapsed time, and its gradient varied after that as its characteristic. Moreover, the transmitted impact stress when the gradient changed (20–25 ms) almost corresponds with the gradient turning point on the compressive strength test result shown in Figure 2. However, in the case of the EST specimen, the transmitted impact stress at this time was greater than that at the inflection point of compressive stress (0.18 MPa) shown in the material testing result. The authors

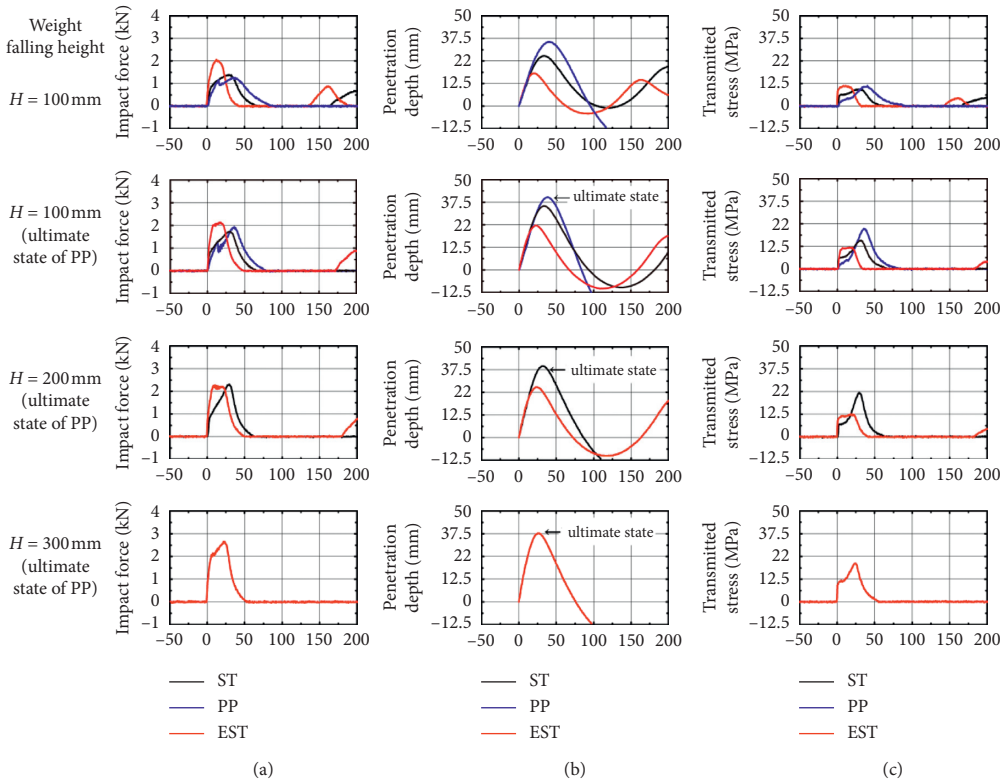

Figure 7: Various time history response waveforms in the case of material without a core slab. (a) Impact force. (b) Weight penetration depth. (c) Transmitted impact stress.

believe that it is necessary to examine this point in future works.

Furthermore, the transmitted impact stress showed a tendency to rise with an increase in the weight fall height H, and the maximum fall heights of the expanded materials showed a tendency to rise suddenly after 25 ms of elapsed time. This was caused by compressive stress increasing rapidly during the process such that strain of the expanded materials reached 75%.

3.2. Transmitted Impact Penetration Stress-Strain Hysteresis Loop. Figure 8 shows the transmitted impact stress-penetration strain hysteresis loops in the case of materials without core slabs. The penetration strain was obtained by dividing the weight penetration depth by the thickness of the expansion material. The figure shows that the area enclosed by the transmitted impact stress-penetrating strain hysteresis loop tends to increase with an increase in fall height. Moreover, the transmitted impact stress was almost constant for the penetration strain up to around 40% whilst the rising gradient of the stress steepens after 50–60%, and its shape is almost similar to that seen in the compressive strength test result shown in Figure 2.

However, in the case of the EST specimen, the transmitted impact stress for penetration strain of up to around 40% is greater than the compressive stress obtained by the material test. Although the above suggests the possibility that speed dependency of EST is high, it is necessary to accumulate data and examine them to verify it in the future [13].

3.3. Damage State of Expanded Material. Figure 5 presents the cut areas of each specimen after the experiment for materials without core slabs. Furthermore, the cut areas are the faces obtained by cutting the materials along the center line, passing through the loading point, as shown in Figure 9. Each sketched cut area in the figure indicates the maximum penetration strain ε_p in the experiment.

From the figure, it can be seen that the residual deformation area increases with an increase in the weight fall height H in either expansion material. The cracking progressing diagonally downward is long, with a widening crack-width. Moreover, although the maximum penetration strain ε_p is greater in the PP specimen than that in the ST specimen, it is superior in the returning performance as the damage is minimal. On the contrary, as the deformation and damage for the same fall height are smaller in the EST specimen than those in the ST specimen, it is superior in the resistance and energy absorption capacity for impacts.

3.4. Transmitted Impact Stress Distribution at the Time of the Maximum Penetration. In Figure 10, transmitted impact stress distributions at the time of the maximum penetration in the case of the materials without core slabs are compared for each fall height H.

The figure shows that the transmitted impact stress right under the loading point reaches its maximum in either specimen, regardless of the fall height. In the case of the ST and PP specimens, the transmitted impact stress of the loading point is prominently high. The tendency that the

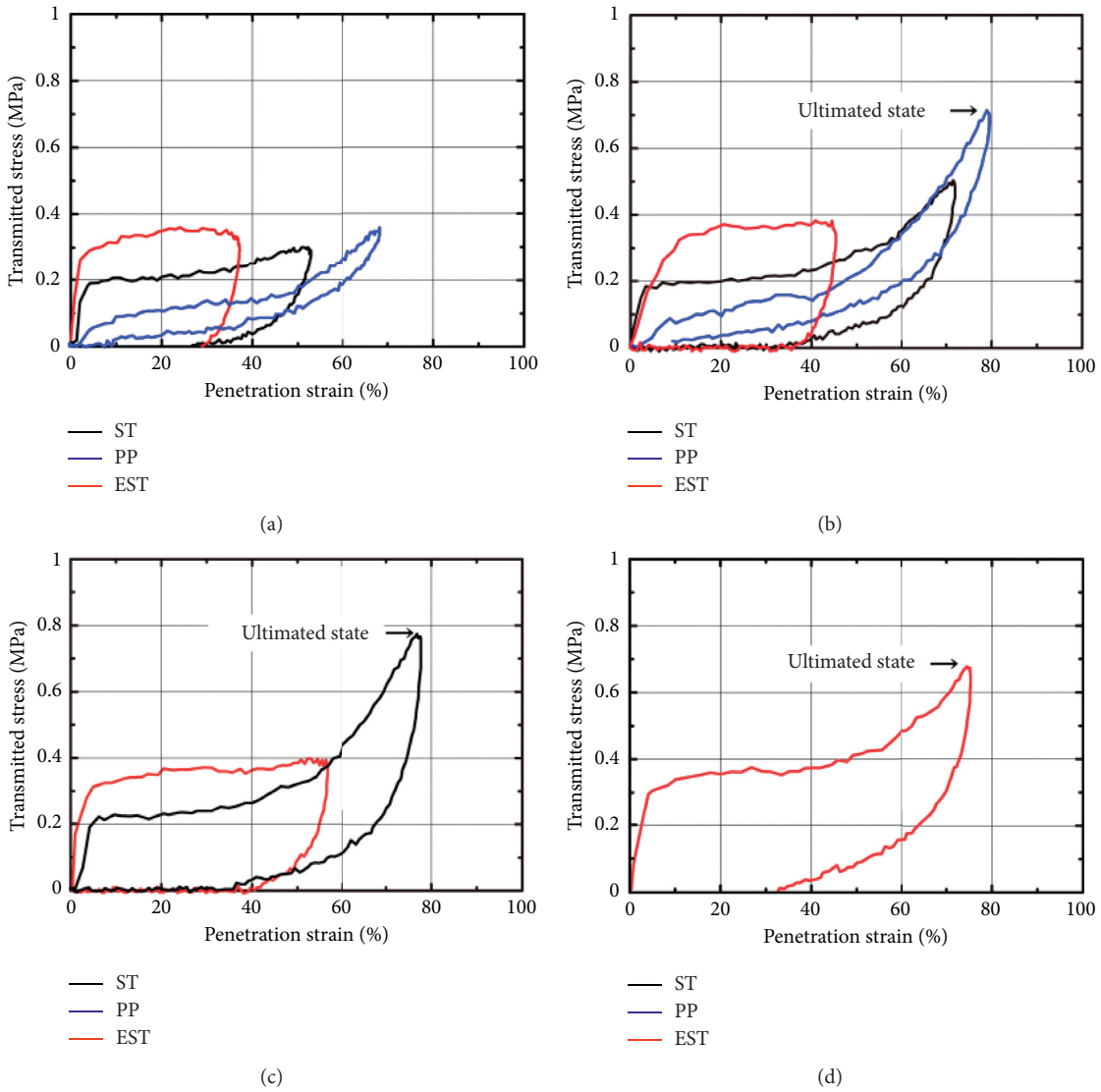

Figure 8: Transmission impact stress-penetration distortion hysteresis loop for materials without a core slab. (a) $H = 100$ mm. (b) $H = 150$ mm. (c) $H = 200$ mm. (d) $H = 300$ mm.

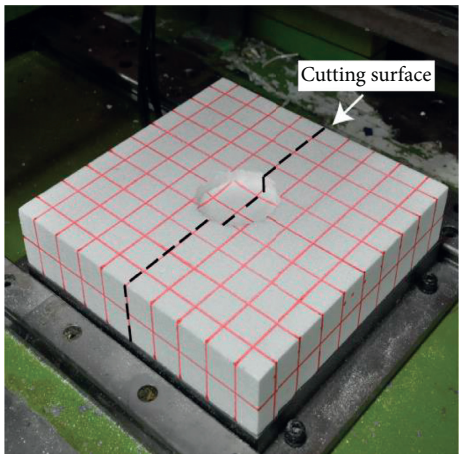

Figure 9: Location of cutting the expanded material.

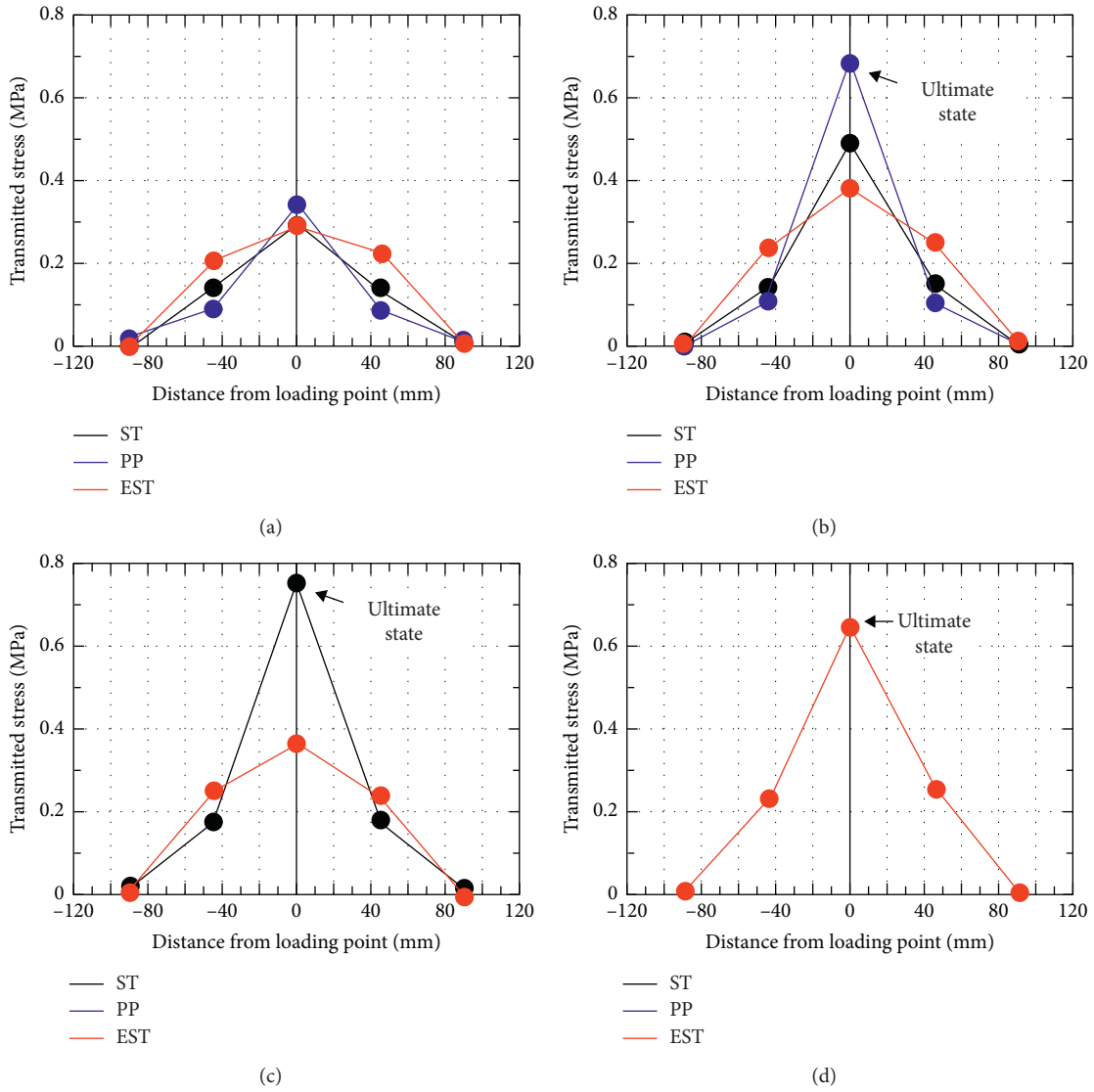

Figure 10: Transmission impact stress distribution at the maximum penetration in the case without core slabs. (a) $H = 100$ mm. (b) $H = 150$ mm. (c) $H = 200$ mm. (d) $H = 300$ mm.

transmitted impact stress at the loading point becomes prominent is evident in the case of $H = 150$ mm, and the PP specimen reaches the ultimate state at this time point. The ST specimen reaches its ultimate state at $H = 200$ mm.

For the EST specimen, the distribution shape of the transmitted impact stress curve displays a pentagon shape with its base wider than the others until $H = 200$ mm, and at $H = 300$ mm, it presents a shape whereby the transmitted impact stress at the loading point becomes prominent. It has been clarified from the above that the transmitted impact stress of the EST specimen with high compressive strength tends to disperse most widely.

4. Experimental Result in the Case with Core Slabs

4.1. Various Response Waveforms. Figure 11 shows the time history response waveform for weight impact force, weight penetration, and transmitted impact stress in the case of the materials with core slabs. It is understood from the figure that the weight impact force, unlike the case without cores, suddenly increased to around 2 kN just after the impact. Then, it was once unloaded and reloaded. This is because the weight collided into the core slab, penetrated it, and deformed the expansion material as mentioned later. Furthermore, the maximum weight impact force for each weight fall height H was smallest in the PP specimen and greatest in the EST specimen, similar to the case without core slabs.

The response waveform for weight penetration and transmitted impact stress presented properties similar to those in the case without core slabs. This is because the core penetrated the expanded material just after the collision and presented deformation behaviors similar to those seen in the case without core slabs. The ST, PP, and EST specimens reached the ultimate state after loading with the fall heights of $H = 400$, 300, and 600 mm, respectively.

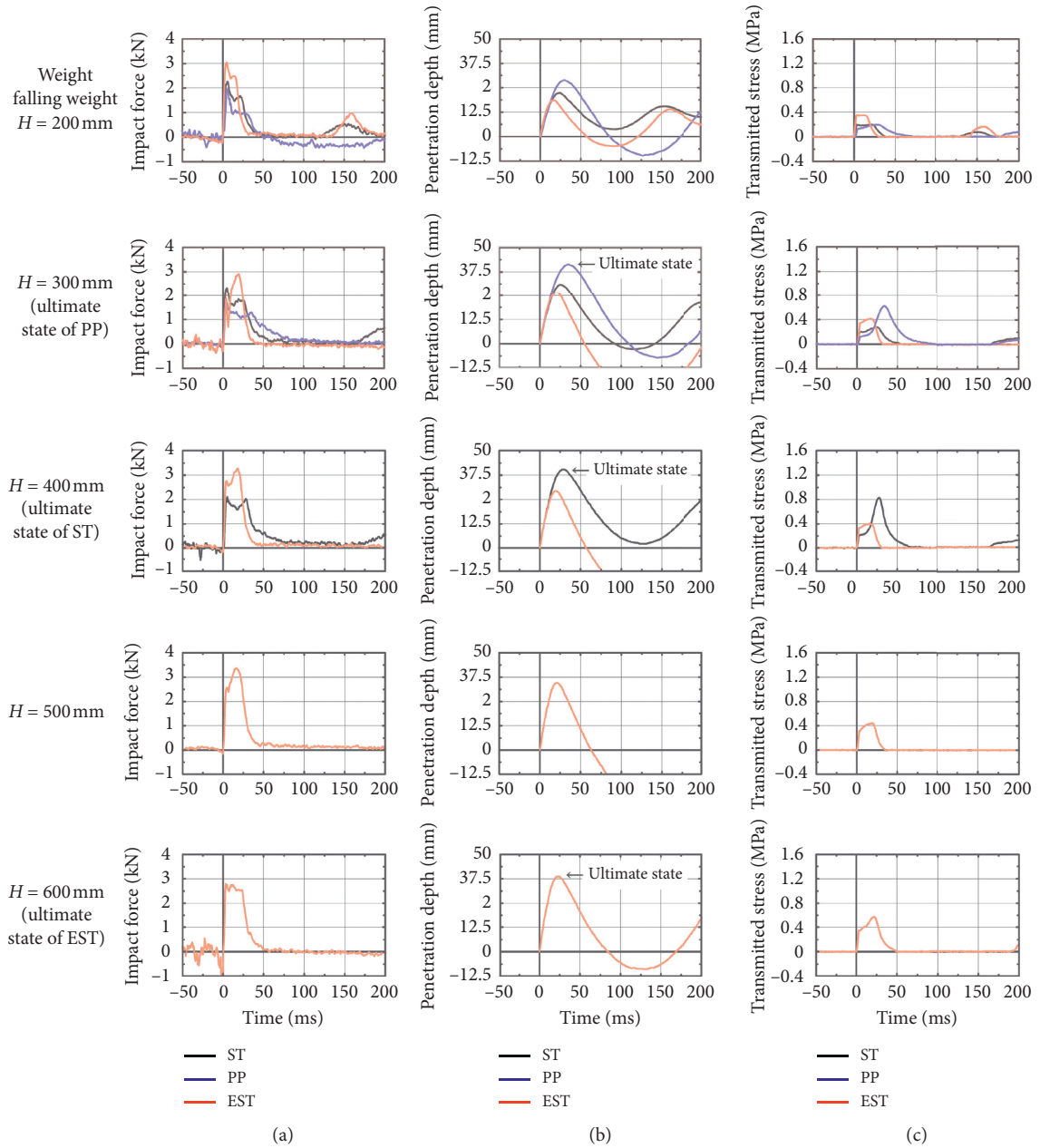

Figure 11: Various time history response waveforms in the case with core slabs. (a) Impact force. (b) Penetration depth. (c) Transmitted impact stress.

4.2. Transmitted Impact Stress-Penetration Strain Hysteresis Loop. Figure 12 presents the transmitted impact stress-penetration strain hysteresis loops in the case of the materials with core slabs. The penetrating strain was obtained by dividing weight penetration by the thickness of expanded material, without regard to the core thickness. This is because the destruction properties showed that the compressive deformation of the core was quite small.

The figure shows that transmitted impact stress-penetration strain hysteresis loops create a large loop as the fall height H increases, similar to the case without core slabs. The initial gradients are lower than those in the case without core slabs. This is because the transmitted impact stress was dispersed by core slabs and the transmitted impact stress right under the loading point decreases.

Moreover, the hysteresis loops with a penetrating strain after 20% present properties that are similar to those obtained by the abovementioned material testing result. This was caused by the energy absorption characteristics that were almost similar to the case without core slabs after the core penetrated the material.

4.3. Damage State of Core and Expansion. Figure 13(a) depicts core slab surface, Figure 13(b) core slab back side, Figure 13(c) expanded material surface after removing core slabs, and Figure 13(d) collapsed state of expanded material after the experiment of the C-ST-H400 specimen. Figures 13(a) and 13(b) show that the core slabs had holes with diameter that is almost equal to that of the weight tip,

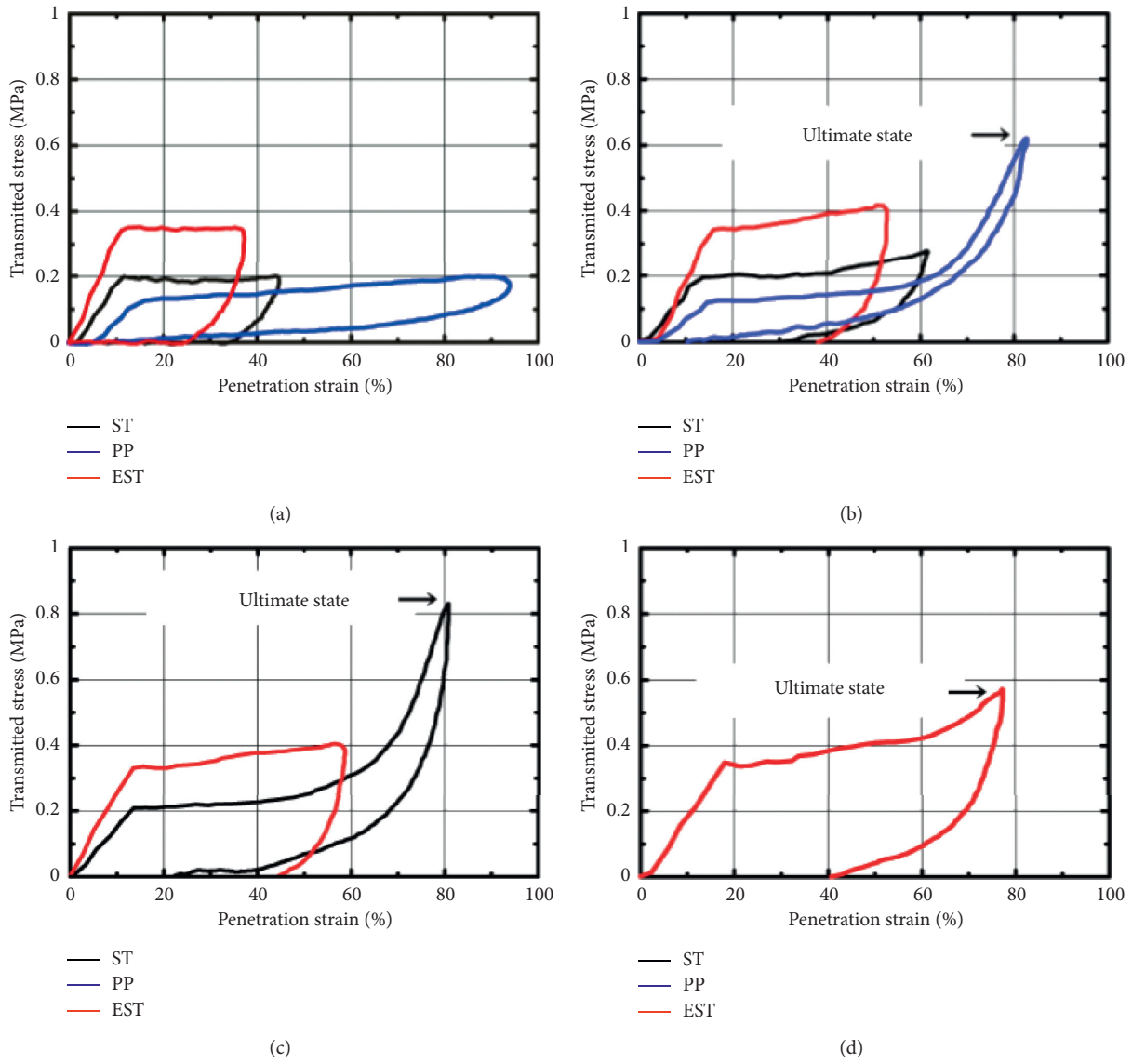

Figure 12: Transmission impact stress-penetrating distortion hysteresis loop in the case with a core slab. (a) $H = 200$ mm. (b) $H = 300$ mm. (c) $H = 400$ mm. (d) $H = 500$ mm. (e) $H = 600$ mm.

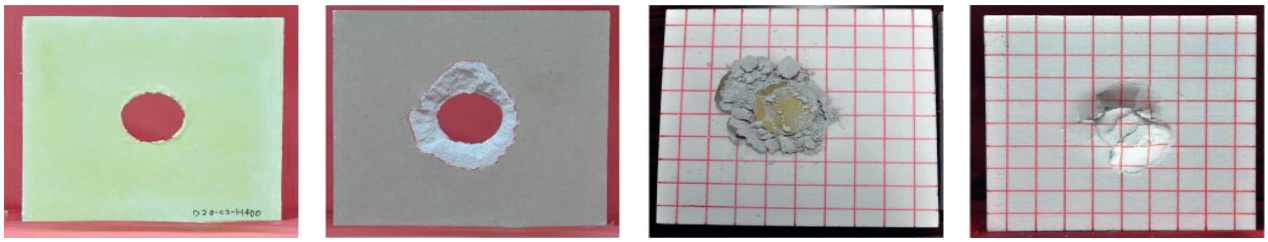

Figure 13: Damage state of the core slab and expanded material of the C-ST-H400 specimen after experiment. (a) Core slab surface. (b) Bottom surface of the slab. (c) Foam material surface after removing the slab. (d) Penetration condition of foam material.

reaching to penetrating shear fracture. Moreover, Figure 13(c) presents a penetrating shear cone separated from the cone on the upper side of the expansion material. Moreover, it is understood from Figure 13(d) that the expansion material was compressively deformed in a wider range than the weight tip diameter due to the influence of penetrating shear

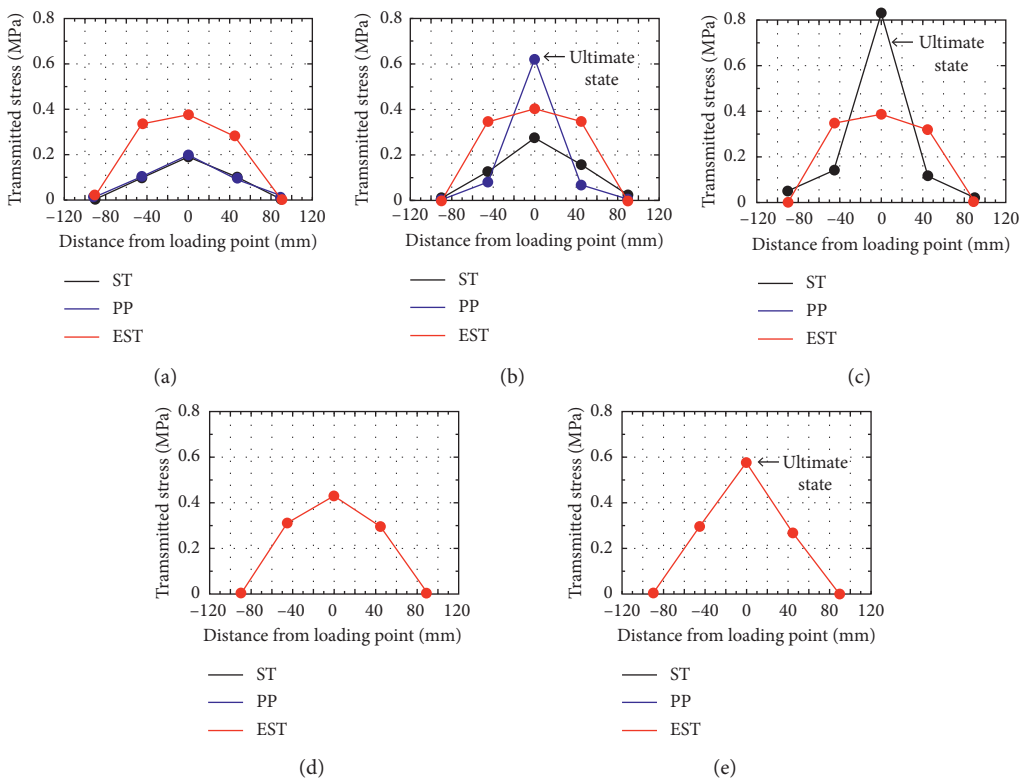

Figure 14: Transmitted impact stress distribution at the time of the maximum penetration with the core slab. (a) $H = 200$ mm. (b) $H = 300$ mm. (c) $H = 400$ mm. (d) $H = 500$ mm. (e) $H = 600$ mm.

fractures of the core slab. Such a tendency was seen in the weight fall impact test of a two-layered absorption system consisting of the existing RC slab and EPS [17].

Figure 6 shows cut area of the expanded material after the experiment. The figure indicates that residual deformation area of the expanded material is greater in the case of ST and EST specimens than in the case without core slabs shown in Figure 5. This is because the impact force was dispersed by the effect of core slabs. This result indicates that the energy absorption capacity of the expanded materials is demonstrated effectively by installing cores, regardless of the type of expanded materials.

Furthermore, in the case without core slabs, ST, PP, and EST specimens reached the ultimate states at $H = 200$, 150, and 300 mm, respectively, and in the case with core slabs, they reached the ultimate states at $H = 400$, 300, and 600 mm, respectively. This result indicates that energy absorption capacity was doubled when core slabs were layered in this experiment, regardless of the expansion materials. As the energy absorption capacity was doubled by core slabs rather than additively increased, it has been demonstrated that the effect of energy absorption capacity was improved by installing core slabs more effectively with greater compressive strength characteristics.

4.4. Transmitted Impact Stress Distribution at the Time of the Maximum Penetration. In Figure 14, transmitted impact stress distribution at the time of the maximum penetration in the case with core slabs is compared for each fall height H.

The results indicate that the transmitted impact stress distribution of the EST specimen displays a pentagon shape with an extended base in the case of the fall height $H = 300$ mm, similar to the case of the core slab with $H = 100$ mm (Figure 10(a)); in the case of the ST and PP specimens, the transmitted impact stress at the loading point tends to be prominently high. Furthermore, the PP specimen reached the ultimate state at this time point and the ST specimen reached its ultimate state at $H = 400$ mm.

On the other hand, in the case of the EST specimen, the transmitted impact stress distribution was in a pentagon shape with an extensive base until $H = 500$ mm, and in triangle shape at $H = 600$ mm. The ESP specimen reached its ultimate state at $H = 600$ mm.

The results clarify that the distribution range of the transmitted impact stresses for the same fall height became most extensive in the case of the EST specimen, which has the highest compressive strength in this study.

5. Estimation of the Maximum Penetration Strain Based on Coefficient of Stress Dispersion

5.1. Coefficient of Stress Dispersion. Table 3 shows a list of experimental results of energy balance in this experiment. Here, the input energy E_k was calculated with measured impact velocity. Moreover, the absorbed energy E_{a1} of the expanded materials right under the weight was calculated as shown below based on the hysteresis loops of transmitted

Table 3: List of experimental results of energy balance.

Name of specimen	Presence of core slab	Type of expanded material	Falling height (mm)	Input energy E_k (J)	Absorbed energy of expanded material right under the weight E_{a1} (J)	Coefficient of stress dispersion $\alpha = E_k/E_{a1}$
N-ST-H50	Without core slab	ST	50	9.77	9.5	1.0
N-ST-H100			100	19.7	16.6	1.2
N-ST-H150			150	30.3	25.8	1.2
N-ST-H200			200	39.1	36.5	1.1
N-PP-H50		PP	50	9.34	6.3	1.5
N-PP-H100			100	19.7	14.5	1.4
N-PP-H150			150	30.3	26.8	1.1
N-EST-H50		EST	50	9.34	10.0	1.0
N-EST-H100			100	19.7	17.0	1.2
N-EST-H150			150	32.9	20.5	1.6
N-EST-H200			200	39.1	27.9	1.4
N-EST-H300			300	65.5	43.2	1.4
C-ST-H200	With core slab	ST	200	42.9	10.4	3.8
C-ST-H300			300	58.4	16.7	3.5
C-ST-H400			400	73.9	32.0	2.5
C-PP-H200		PP	200	39.1	10.4	3.8
C-PP-H300			300	65.5	21.3	2.8
C-EST-H200		EST	200	42.9	16.6	2.6
C-EST-H300			300	58.4	22.8	2.6
C-EST-H400			400	84.1	26.8	2.9
C-EST-H500			500	96.5	31.5	3.1
C-EST-H600			600	112.0	38.6	3.0

impact stress and penetrating strain right under the loading point shown in Figures 8 and 12:

$$E_{a1} = S \times H \times A, \tag{1}$$

where S = integration value (MPa) until the maximum penetration strain in the transmitted impact penetrating stress-strain hysteresis loop (see Figure 15), H = expanded material height (mm), and A = area of the bottom face area of the weight (mm^2).

The coefficient of stress dispersion α was obtained by the following equations under the assumption that the input energy E_k is equivalent to the absorbed energy E_a of the entire expanded materials:

$$E_k = E_a = \alpha \times E_{a1},$$
$$\alpha = \frac{E_k}{E_{a1}}. \tag{2}$$

It is understood from these equations that α is physical quantity obtained by dividing the total absorbed energy E_a of the expanded material (= input energy E_k) by the absorbed energy E_{a1} of the expanded material under the weight. Therefore, it is thought that α is evaluable as an index indicating spread of the energy absorption range of the expansion material. Furthermore, energy absorption by core slabs was ignored based on the assumption that it is much smaller than that of the expanded materials. The table shows that the coefficient of stress dispersion α is 1.0–1.6 in the case without core slabs and 2.5–3.8 in the case with core slabs. It has been revealed quantitatively that the coefficient of stress dispersion α was increased by core slabs and the expanded materials absorbed energy effectively in a wide range.

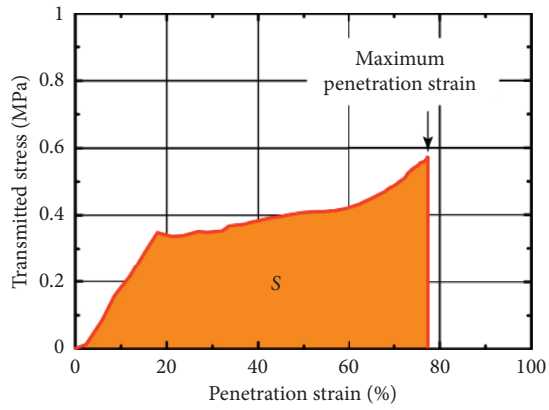

Figure 15: Integral values to the maximum penetration strain.

An estimation of the coefficient of stress dispersion α geometrically using the weight radius R and core thickness t, based on the assumption that the core punching shear fractures at 45 degrees, is shown in Figure 16, and it is expressed by the following equation:

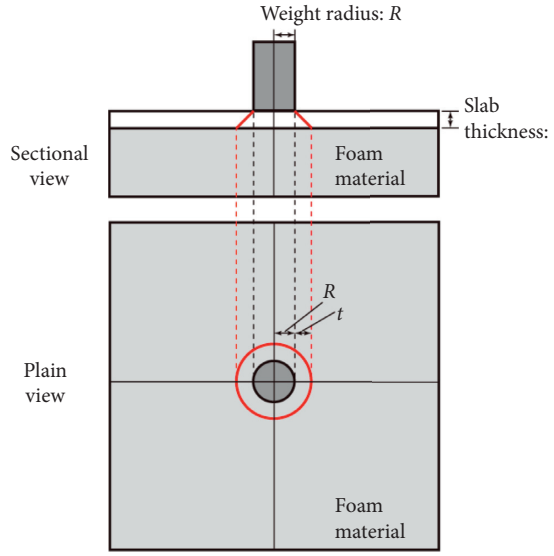

Figure 16: Conception diagram of the punching shear fracture of the core slab (in the case that diagonal tension cracking the angle of the core slab is 45 degrees).

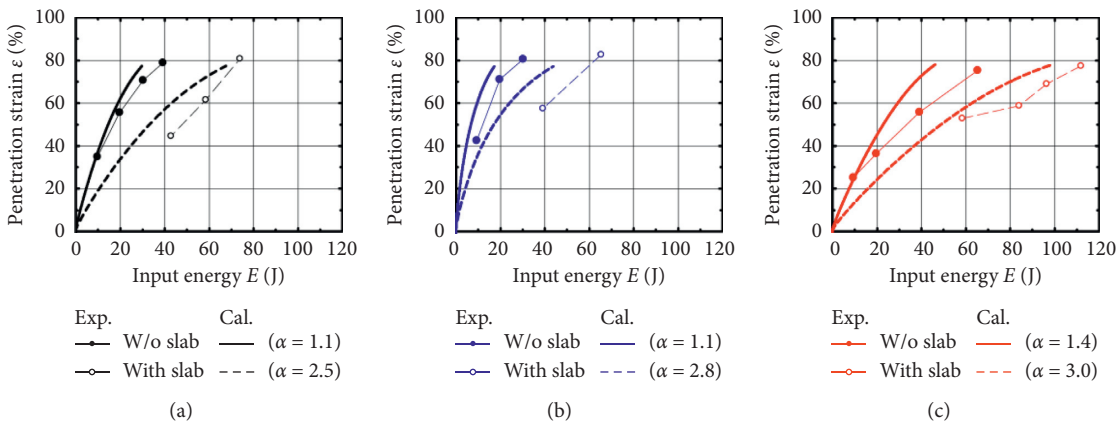

Figure 17: Weight penetration-input energy relationship. (a) ST. (b) PP. (c) EST.

$$\alpha_p = \frac{\pi (R + t)^2}{\pi R^2} = \left(1 + \frac{t}{R}\right)^2, \quad (3)$$

where α_p is the theoretical coefficient of stress dispersion for the punching shear model.

In this experiment, as the weight radius $R = 30$ mm and core thickness $t = 12.5$ mm, the coefficient of the stress dispersion $\alpha_p = 2.01$. The above suggests that transmitted impact stress disperses more widely than the assumptions, as outlined in Figure 16.

5.2. Estimation of the Maximum Penetration Strain. Here, the maximum weight penetration is calculated and compared with the experimental result, in accordance with the compression stress-strain relation (see Figure 2) based on the coefficient of the stress dispersion α and material testing. Furthermore, values at the time of the maximum input energy were used for the coefficient of the stress dispersion α of each specimen.

The experimental results of the maximum penetration strain ε_p for each input energy E_k are plotted in Figure 17 and compared with the penetration strain-input energy curve obtained by the calculation result. Here, the input energy E for the arbitrary penetration strain ε was obtained by the following equation and is expressed as an ε–E curve in the calculation result:

$$E = \alpha \times S_a(\varepsilon) \times H \times A. \quad (4)$$

Here, $S_a(\varepsilon)$ represents integral values to the arbitrary strain ε in the compression stress-strain relationship based on the material testing results (see Figure 2). The figure shows that penetration strain for the same input energy is smaller in the case with core slabs than in the case without them in both experimental and calculation results in either specimen. Moreover, the penetration strain with the same

input energy is smallest and superior in energy absorption capacity to the EST specimen.

Comparison of the experiment and calculation results shows that the calculation result is greater than the experimental result by around 30% in some cases, whilst on the other hand there is an increased tendency of the penetration strain to increase the input energy seen in both cases.

Therefore, the maximum penetration strain ε_p can be evaluated by appropriately setting the stress dispersion coefficient α corresponding to various absorbents and core slabs and using the relationship between compressive stress and strain based on material tests. The safety factor under the conditions of this study is about 30%.

In the case that expanded materials with high compressive strength such as the EST specimen are used, transmission impact force rises accordingly. Therefore, it is necessary to design absorption materials considering load-carrying capacity of existing rock shed. Moreover, in order to improve accuracy of the penetration evaluation method proposed in this paper, it is necessary to (1) clarify the difference between the material testing result and impact-loading test result in the stress-strain relation and (2) evaluate α corresponding to various expanded materials.

6. Conclusion

In this study, falling-weight impact-loading tests with various fall heights were performed for examining the absorption performance of various expansion materials. We examined the case wherein core slabs were layered for an effective utilization of the absorption performance of expanded materials. The findings of this study are summarized as follows:

(1) The transmitted impact stress-penetration strain curves right under the loading points of various expanded materials exhibit properties that are similar to those obtained from the results of the material testing. However, in the case of expanded materials with high compressive strengths, the compressive stress tends to be higher than that observed in the results of material testing.

(2) In the case of expanded materials with high compressive strengths, with and without core slabs, the distribution of the transmitted impact stress and energy absorption capacity is large.

(3) In this experiment, the energy absorption capacity doubles when core slabs are layered, regardless of the type of expansion material. This indicates that expansion materials with high compressive strengths may result in higher improvements in the energy absorption capacity by using layered core slabs.

Data Availability

All the data used to support the findings of this study are available from the corresponding author upon request.

Conflicts of Interest

The authors declare that there are no conflicts of interest regarding the publication of this paper.

Acknowledgments

For promoting this research, the undergraduate and graduate students of Structural Mechanics Laboratory, Graduate School of Muroran Institute of Technology, received a significant amount of support for the loading experiments, data arrangement, etc. This work was supported by JSPS KAKENHI (19H02394).

References

[1] J. Mysiak, S. Castellari, B. Kurnik et al., "Brief communication: strengthening coherence between climate change adaptation and disaster risk reduction," *Natural Hazards and Earth System Sciences*, vol. 18, no. 11, pp. 3137–3143, 2018.

[2] J. Borella, M. Quigley, Z. Krauss et al., "Geologic and geomorphiccontrols on rockfall hazard: how well do pastrockfalls predict future distributions?" *Natural Hazards and Earth System Sciences*, vol. 19, no. 10, pp. 2249–2280, 2019.

[3] A. Volkwein, K. Schellenberg, V. Labiouse et al., "Rockfall characterisation and structural protection - a review," *Natural Hazards and Earth System Sciences*, vol. 11, no. 9, pp. 2617–2651, 2011.

[4] Y. Kurihashi, M. Komuro, M. Schubert, R. Custer, and K. Schellenberg, "Failure probability for extreme load cases evaluated by FE calculations–A case study for the rockfall protection gallery," *Proceedings of IABSE Symposium*, vol. S27, pp. 36–42, 2018.

[5] F. Bourrier, N. Eckert, F. Nicot, and F. Darve, "Bayesian stochastic modeling of a spherical rock bouncing on a coarse soil," *Natural Hazards and Earth System Science*, vol. 9, no. 3, pp. 831–846, 2009.

[6] B. Pichler, C. Hellmich, and H. A. Mang, "Impact of rocks onto gravel Design and evaluation of experiments," *International Journal of Impact Engineering*, vol. 31, no. 5, pp. 559–578, 2005.

[7] F. Calvetti and C. di Prisco, "An uncoupled approach for the design of rockfall protection tunnels," *Structural Engineering International*, vol. 19, no. 3, pp. 342–347, 2009.

[8] ASTRA, "Impacts due to stone chipping on protective galleries," Tech. Rep., Swiss Federal Print and Material Center, Bern, Switzerland, 2008.

[9] Japan Road Association, *Manual for Anti-impact Structures against Falling Rocks*, Japan Road Association, Tokyo, Japan, 2000.

[10] Z.-L. Wang, Y.-C. Li, and J. G. Wang, "Numerical analysis of attenuation effect of EPS geofoam on stress-waves in civil defense engineering," *Geotextiles and Geomembranes*, vol. 24, no. 5, pp. 265–273, 2006.

[11] S. Zarnani and R. J. Bathurst, "Numerical parametric study of expanded polystyrene (EPS) geofoam seismic buffers," *Canadian Geotechnical Journal*, vol. 46, no. 3, pp. 318–338, 2009.

[12] N. Kishi, O. Nakano, H. Mikami, K. G. Matsuoka, and N. Sugata, "Field test on shock absorbing effect of three-layered absorbing system," *Proceedings of SMiRT*, vol. 12, pp. 357–362, 1993.

[13] S. Ouellet, D. Cronin, and M. Worswick, "Compressive response of polymeric foams under quasi-static, medium and

high strain rate conditions," *Polymer Testing*, vol. 25, no. 6, pp. 731–743, 2006.

[14] E. O. Umud and A. Gunay, "Hydrostatic compression of anisotropic low density polymeric foams under multiple loadings and unloadings," *Polymer Testing*, vol. 30, no. 7, pp. 737–742, 2011.

[15] International Organization for Standardization, *ISO 844: 2004, Rigid Cellular plastics–Determination of Compression Properties*, International Organization for Standardization, Geneva, Switzerland, 2004.

[16] Japanese Industrial Standard, *JIS A 6901: 2014, Gypsum Boards*, Japanese Industrial Standard, Tokyo, Japan, 2014.

[17] R. Kawase, N. Kishi, H. Nishi, Y. Ushiwatari, and K. Karita, "Weight impact test of rockfall retaining-wall connected with steel piled foundation by using H-section steel," *Journal of Structural Engineering*, vol. 56A, pp. 1113–1122, 2010, in Japanese.